Polarized neutron capture on ^{13}C

M. C. Wright, H. Kitazawa,* N. R. Roberson, and H. R. Weller
Duke University and Triangle Universities Nuclear Laboratory, Duke Station, Durham, North Carolina 27706

M. Jensen and D. R. Tilley
North Carolina State University, Raleigh, North Carolina 27695
and Triangle Universities Nuclear Laboratory, Duke Station, Durham, North Carolina 27706

(Received 19 October 1984)

The 90° cross section yield curve for the $^{13}C(n,\gamma_0)^{14}C$ reaction has been measured from $E_n(E_x)=5.6(13.4)$ to 17.0(24.0) MeV. Angular distributions of cross section and analyzing power were measured at seven energies spanning this excitation region. In addition, the fore-aft asymmetry and 90° analyzing power were measured as a function of energy from $E_n=7.75$ to 17.0 MeV. The data were compared to direct-semidirect model calculations which included the isovector dipole and isoscalar electric quadrupole transitions. These comparisons indicate the presence of two narrow $M1$ resonances at $E_x=16.5$ and 17.5 MeV and that $\sigma(E2)$ is less than 2% of the total capture cross section in the energy region of this experiment.

I. INTRODUCTION

The study of radiative capture with polarized nucleons has proven to be useful in determining the reaction matrix elements associated with the ground-state channel of the giant dipole resonance (GDR).[1] In addition, these studies are of interest in that they can provide information on non-$E1$ strength ($M1$ and $E2$) in this excitation region.[1,2] For the particular spin sequence $J_{\text{target}}=\frac{1}{2}$ and $J_{\text{residual}}=0$, or vice versa, only two complex transition amplitudes contribute for each multipole. If $E1$, $M1$, and $E2$ radiations are present, there are 11 reaction parameters (six real amplitudes and five relative phases) and, as will be discussed below, the problem is underdetermined. It is therefore necessary to employ a reaction model in interpreting the results.

A frequently used model for fast-nucleon capture is the direct-semidirect (DSD) model.[3,4] In this model the transition amplitude is expressed as the sum of two terms. The first is called the direct term and corresponds to the situation in which the incoming nucleon undergoes a radiative transition from its scattering state into a single-particle bound state. The second is the semidirect term which represents the case of the incoming nucleon inelastically exciting the target nucleus into a collective state while capturing into the same single-particle bound state as in the direct process. The DSD model has been used extensively and with success to explain the results of radiative capture measurements in p-shell nuclei.[1,2]

One of the complicating factors with the (p,γ) reaction is the presence of the "direct $E2$ capture" cross section which tends to obscure any collective $E2$ strength.[1,5] A potential advantage[6] of polarized neutron capture over proton capture is that the direct $E2$ capture amplitude is scaled by the recoil effective charge[7] which for neutrons is negligible except for the lightest nuclei. Consequently, for the (n,γ) reaction, any observed $E2$ radiation can be attributed to collective (semidirect) strength.

In the present paper we shall present the results of our investigation of the $^{13}C(\vec{n},\gamma_0)^{14}C$ reaction. The 90° cross section yield curve was measured for neutron energies from 5.6 to 17.0 MeV. Angular distributions of cross section, $\sigma(\theta)$, and analyzing power, $A_y(\theta)$, have been measured with both polarized and unpolarized neutrons at seven energies which encompass the giant resonance region. In addition, $A_y(90°)$ was measured at 17 energies and the fore-aft asymmetry, a_s, at 11 energies from $E_n=7.75$ to 17 MeV. The experimental results are compared with the predictions of direct-semidirect model calculations which assume that $E1$, $M1$, and $E2$ radiations are present in the reaction. The results of this comparison are (1) that there is little evidence from the angular distribution data for the presence of any significant collective $E2$ strength in the (γ,n_0) channel, and (2) that there is agreement with the energy dependence of $A_y(90°)$ and a_s only when two $M1$ resonances at excitation energies of 16.7 and 17.5 MeV are included in the analysis.

II. EXPERIMENTAL DETAILS

A detailed explanation of the experimental apparatus has been published elsewhere[8] and only the salient features will be given here.

The $^2H(d,n)^3He$ reaction was used to produce the neutron flux. A 2.54 cm long gas cell with a 5.65 mg/cm^2 Havar foil entrance window was filled with deuterium, and the pressure in the cell was maintained at 5 atm for $E_n<9.1$ MeV and at 6 atm for $E_n>9.1$ MeV. The energy spread of the neutrons varied from 400 keV at $E_n=7.75$ MeV to 180 keV at $E_n=17.0$ MeV. Measurements[9] of the 0° neutron yield made with a proton recoil counter agreed within a few percent with the values calculated from the integrated beam current, deuterium gas cell pressure, and previously measured $^2H(d,n)^3He$ cross sections.[10]

Polarized neutrons were obtained by bombarding the

deuterium gas cell with polarized deuterons. The neutron polarization was calculated from the beam polarization by using the polarization-transfer coefficients previously reported by Lisowski *et al.*[11] In the present work the vector and tensor polarization of the deuteron beam were equal and typically 0.68 ± 0.02 as measured by the quench-ratio method.[12] The resulting neutron-beam polarization was typically 0.60 ± 0.04. A pulsed deuteron beam having a pulse width on target of approximately 2 nsec was used for both unpolarized and polarized neutron measurements. Beam currents ranged from 60 to 90 nA for the polarized deuteron beams and 200 to 350 nA for the unpolarized case.

The target consisted of 32.4 g of 96% isotopically enriched ^{13}C pressed into a thin-walled Lucite cylinder 3.8 cm high and 3.8 cm in diameter (internal dimensions). An identical empty Lucite cylinder was used for performing target-out measurements. The target was suspended at 0° relative to the beam direction at a distance of 8.9 cm from the center of the target to the center of the deuterium gas cell.

Two γ-ray spectrometers, located on opposite sides of the beam axis, each consisted of a 25.4 cm by 25.4 cm NaI(Tl) crystal mounted inside a well-type plastic (NE110) scintillator anticoincidence shield. The spectrometers were surrounded by 10 cm of lead, and the lead was surrounded by 20 cm of paraffin doped with lithium carbonate. Additional shielding for thermal neutrons in the form of 0.16 cm thick cadmium sheets or 1.25 cm of plastic doped with boron carbide was located between the lead and paraffin. Tungsten "shadow bars" were placed to shield each spectrometer from the direct neutron flux produced in the gas cell. To further minimize the effects of neutron induced background in the NaI crystal, prompt γ-ray events were selected by applying a time-of-flight criterion relative to the pulsed beam.

The standard fast electronics used to operate these spectrometers serve three main functions. The first and primary function is to reduce the probability of pulse pileup.[13] The second function is to detect coincidence events in the NaI crystal and shield, and the third is to generate a time-of-flight spectrum. Since the counting rates in this experiment were low, the shield energy discriminators were operated with a high threshold. This resulted in an increase in the detection efficiency but with some loss in γ-ray energy resolution. In this mode the efficiency is $(27\pm2)\%$ for 15 MeV γ rays. The method used to determine the efficiencies of these spectrometers as a function of γ-ray energy has been discussed in detail in Ref. 8.

A 90° γ-ray spectrum obtained at $E_n=9.6$ MeV with the ^{13}C target is shown in Fig. 1. The data in the figure represent those events that were detected in the NaI crystal without a coincident event in the shield and that also occurred with the proper time-of-flight criterion.

III. DATA ANALYSIS

The yields for the γ-ray transitions to the ground state were determined by first fitting the γ-ray energy spectra with a standard line shape.[8] From these fits the smooth energy dependence of the widths (FWHM) were determined as well as the locations of the centroids of the peaks. The number of counts in the full-energy peaks were then obtained directly from the data with a summing region extending from 1.0 width below the centroid to 1.1 widths above the centroid. Target-out spectra were summed using the same region and, after normalization, were subtracted from the data. The resulting sums were normalized to the same integrated beam current and corrected for dead time and accidental coincidence effects.

In order to obtain absolute values for the cross sections, it is necessary to correct for the finite extent of the neutron source and size of the target and detector. The angular distributions of cross section for the $^2H(d,n)^3He$ reaction were taken from Drosg.[10] The neutron flux, which is forward peaked, was then averaged over the volume of the gas cell and ^{13}C sample. Corrections were also made for neutron multiple scattering. These corrections were calculated with a computer code which uses Monte Carlo techniques. Figure 2 shows examples of the multiplicative correction factors as a function of angle for $E_n=10.2$ MeV. The curves labeled σ, σ^+, and σ^- give the correc-

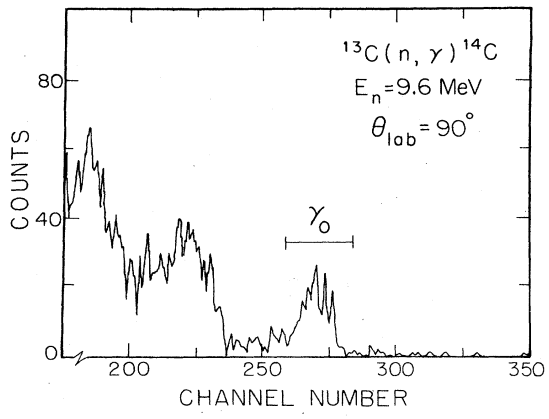

FIG. 1. A 90° γ-ray spectrum from the $^{13}C(n,\gamma_0)^{14}C$ reaction at $E_n=9.6$ MeV.

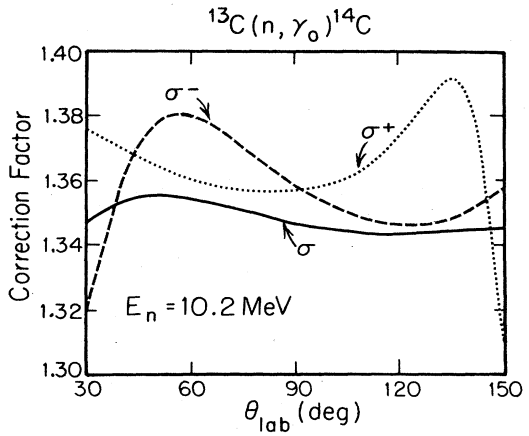

FIG. 2. Example of finite geometry multiplicative correction factors as a function of angle. The curves labeled σ, σ^+, and σ^- correspond to unpolarized beam, polarized beam with spin up, and polarized beam with spin down, respectively.

tion factors which were obtained for the case of an unpolarized beam, a polarized beam with spin up, and a polarized beam with spin down, respectively. The correction factors were applied to the cross sections previously normalized to the 0° neutron flux. These calculations show that the relative corrections to the angular distribution data are small. On the other hand, the correction to the 90° yield curve data is substantial and varies (almost linearly) from about 1.24 at $E_n=7.75$ MeV to 1.46 at 13.0 MeV. For neutron energies outside this range a linear extrapolation was used to obtain the correction factors.

The fore-aft asymmetry measurements were made by placing one of the detectors at 55° while the other was at 125°, and then exchanging the positions and repeating the measurement. The fore-aft asymmetry is then given by the expression

$$a_s=\frac{q-1}{q+1},$$

$$q^2=\frac{L_{55}R_{55}}{L_{125}R_{125}},$$

where L_{55} (R_{55}) and L_{125} (R_{125}) are the yields when the left (right) detector is at 55° and 125°, respectively.

The angular distributions of center-of-mass cross section were fitted by an expansion of Legendre polynomials given by

$$\sigma(\theta)=A_0\left[1+\sum_{k=1}^{3}a_kP_k(\cos\theta)\right].$$

In addition, the fits were made subject to the constraint that the a_k coefficients agree with the measured values of the fore-aft asymmetry, a_s. The errors of a_s were allowed to contribute to the errors of the a_k coefficients.

The fits to the angular distributions reported in this work were made through $k=3$. The inclusion of $k=4$ terms was not statistically justified and did not significantly change the values of the lower order a_k coefficients.

The 90° analyzing power yield curve was measured by placing each of the two detectors at 90°. The values of $A_y(90°)$ were calculated from the expressions

$$A_y(90°)=\frac{1}{P}\left[\frac{r-1}{r+1}\right],$$

$$r^2=\frac{L_+R_-}{L_-R_+},$$

where L_+ (R_+) and L_- (R_-) are the yields for the left (right) detectors for spin up and spin down, respectively, and P is the beam polarization.

The angular distributions of analyzing power were measured before the second γ-ray spectrometer was installed. For the case of a single spectrometer the analyzing power was determined from the expression

$$A_y(\theta)=\frac{1}{P}\left[\frac{N_+-N_-}{N_++N_-}\right],$$

where N_+ and N_- are the yields for the same integrated beam current for spin up and spin down, respectively. The product $A_y(\theta)\sigma(\theta)/A_0$ was fitted by an expansion in associated Legendre polynomials given by

$$\frac{A_y(\theta)\sigma(\theta)}{A_0}=\sum_{k=1}^{3}b_kP_k^1(\theta).$$

These fits were constrained so that the b_k coefficients were consistent with the values of $A_y(90°)$ which were obtained with the two-detector system. The inclusion of $k=4$ terms was not statistically justified and did not significantly change the values of the lower order b_k coefficients.

IV. RESULTS AND DISCUSSION

The 90° cross section yield curve for the $^{13}C(n,\gamma_0)^{14}C$ reaction was measured in 200 keV steps for incident neutron energies from 5.6 to 13.0 MeV and at selected energies between 13.0 and 17.0 MeV. The results are shown in Fig. 3. These neutron energies correspond to excitation energies in ^{14}C from 13.4 to 24.0 MeV. The absolute cross sections given here were obtained using finite-size correction factors, detector efficiencies, target mass, and integrated beam currents, and are estimated to have a total uncertainty of ±20%. The total capture cross section, $\sigma(n,\gamma)=4\pi A_0$, was determined by multiplying the 90° cross sections by the factor $4\pi A_0/\sigma(90°)$. The values of $A_0/\sigma(90°)$ were determined from a smooth curve drawn through the seven experimental values of this ratio obtained from the measured angular distributions. The principle of detailed balance was used to convert the (n,γ_0) cross sections to (γ,n_0) cross sections which were then integrated over the experimental energy range by assuming smoothly varying cross sections. The $^{14}C(\gamma,n_0)^{13}C$ channel exhausts approximately 14% (29 mb MeV) of the classical dipole sum[14] for the excitation energy range of 13.4 to 24.0 MeV.

The total and partial photonuclear cross sections of ^{14}C

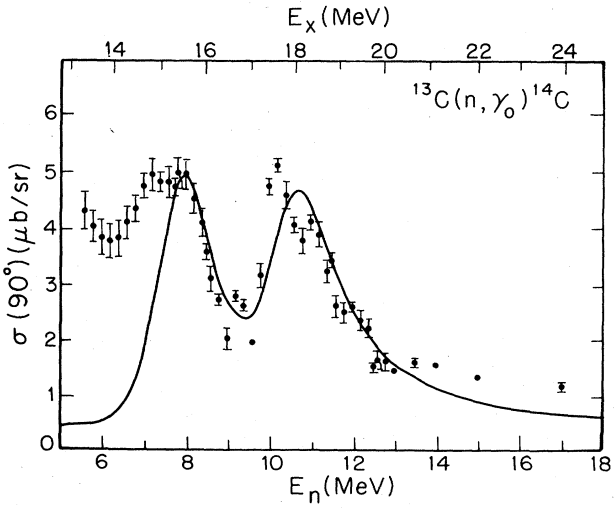

FIG. 3. The 90° cross section versus incident neutron energy for the $^{13}C(n,\gamma_0)^{14}C$ reaction. The curves represent DSD model calculations (see the text). The error bars represent only the statistical uncertainties associated with the data points.

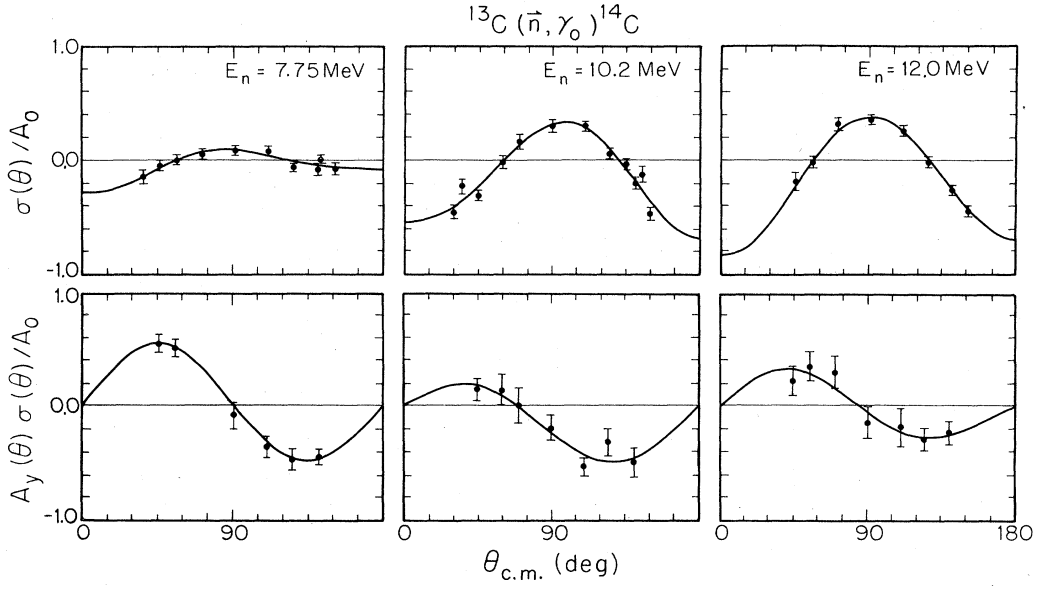

FIG. 4. A sample of the angular distributions of cross section and analyzing power for the $^{13}C(\vec{n},\gamma_0)^{14}C$ reaction. The curves are the result of the polynomial fits to the data (see the text). The error bars represent only the statistical uncertainties associated with the data points.

have been calculated using a bound-state shell model combined with the R-matrix theory by Kissener *et al.*[15] These authors found that the calculated (γ,n_0) cross section is due primarily to the decay of $T=1$ levels near $E_x=(15\pm3)$ MeV, and that the integrated (γ,n_0) cross section from 10 to 25 MeV excitation is about 32 mb MeV (taken from Fig. 9 of Ref. 15). These calculations are in qualitative agreement with the results of this experiment.

A sample of the angular distribution data and polynomial fits is displayed in Fig. 4. Measurements were also made at $E_n=9.2$, 10.0, 11.0, and 13.0 MeV but are not shown. The a_k and b_k coefficients obtained from the polynomial fits to the data are given in Fig. 5. At $E_n=13.0$ MeV, $A_y(\theta)$ was measured at only three angles:

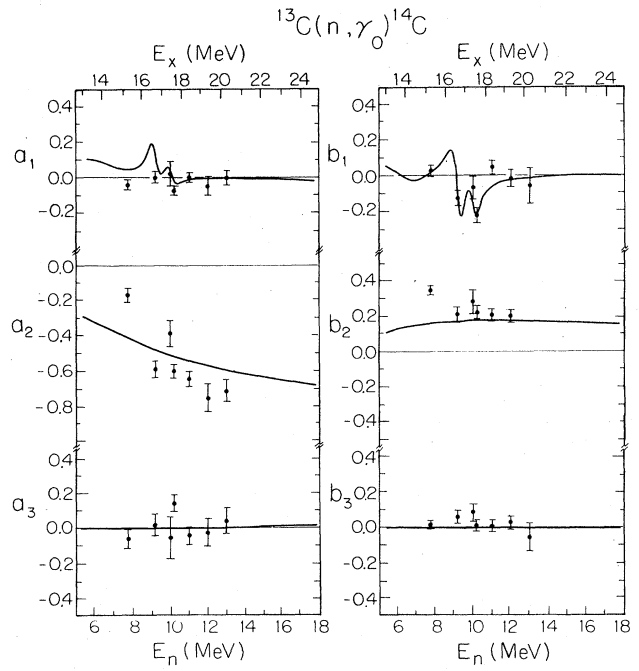

FIG. 5. The a_k and b_k coefficients for the $^{13}C(\vec{n},\gamma_0)^{14}C$ reaction. As discussed in the text, the curves are the results of a DSD model calculation which includes two narrow $M1$ resonances at $E_x=16.5$ and 17.0 MeV. The error bars represent only the statistical uncertainties associated with the data points.

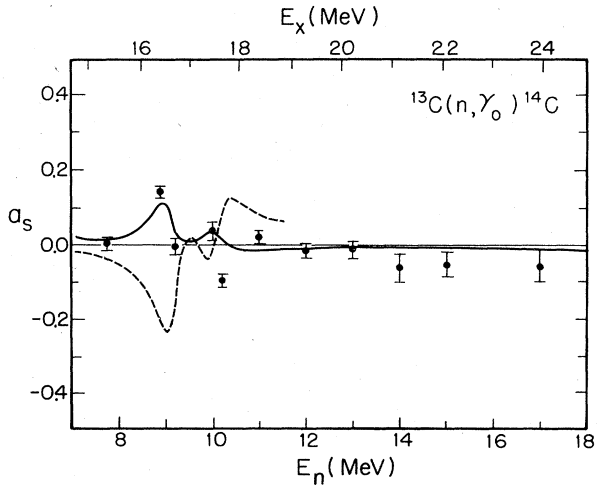

FIG. 6. The fore-aft asymmetry as a function of incident neutron energy for the $^{13}C(n,\gamma_0)^{14}C$ reaction. As discussed in the text, the solid curve represents a DSD model calculation which includes two narrow $M1$ resonances at $E_x=16.5$ and 17.0 MeV, while the dashed curve is the result of replacing the two $M1$ resonances with two isoscalar $E2$ resonances at the same excitation energies. Statistical uncertainties are indicated.

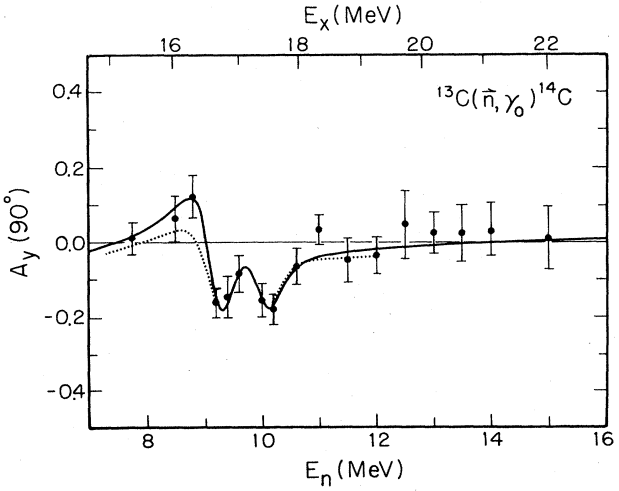

FIG. 7. Same as Fig. 6 for $A_y(90°)$.

90°, 110°, and 125°. Examination of Fig. 5 shows that for E_n above 10.0 MeV, the experimental b_2 coefficients are almost constant and have a value near 0.2. The $A_y(\theta)$ data at $E_n=13.0$ MeV were, therefore, analyzed by fixing $b_2=0.20\pm0.04$ and fitting b_1 and b_3 to the three measured values. The energy dependence of the fore-aft asymmetry and $A_y(90°)$ are shown in Figs. 6 and 7, respectively. The curves given in Figs. 3, 5, 6, and 7 represent DSD model calculations and will be discussed below (Sec. V).

As discussed in the Introduction, the simple spin sequence $J_{\text{target}}=\frac{1}{2}$ and $J_{\text{residual}}=0$ for the $^{13}C(n,\gamma_0)^{14}C$ reaction allows, in general, only two transition matrix elements for each multipole. For the case of $E1$, $E2$, and $M1$ transitions, these complex matrix elements can be written in terms of a real amplitude and phase as

$$s_{1/2}(E1)e^{i\phi_s},\ d_{3/2}(E1)e^{i\phi_d},$$

$$p_{3/2}(E2)e^{i\phi_p},\ f_{5/2}(E2)e^{i\phi_f},$$

and

$$p_{1/2}(M1)e^{i\phi_{p1}},\ p_{3/2}(M1)e^{i\phi_{p3}},$$

respectively, where the terms are labeled (in j-j coupling) by the value of l and j for the incident neutron and by the multipolarity of the emitted radiation.

Although the nonzero values of coefficients other than a_2 and b_2 clearly indicate the presence of non-$E1$ radiation,[1] the majority of the strength in the excitation-energy range studied here is expected to be $E1$, and hence a pure $E1$ analysis of the data should be useful.[1,16] Neglecting all radiations except $E1$ implies that only the a_2 and b_2 coefficients are nonzero. These coefficients can be written in terms of the two $E1$ amplitudes and their relative phase as

$$1.0=s_{1/2}^2+2d_{3/2}^2 \text{ (normalization)},$$

$$a_2=-2s_{1/2}d_{3/2}\cos(\phi_d-\phi_s)-d_{3/2}^2,$$

$$b_2=-s_{1/2}d_{3/2}\sin(\phi_d-\phi_s).$$

These equations can be solved directly to obtain the $E1$ amplitudes and relative phase, and two solutions are obtained at each energy. The results of this analysis are shown in Fig. 8, where the normalization for plotting purposes is $\sigma(s_{1/2})+\sigma(d_{3/2})=100\%$ and $\sigma(d_{3/2})=2d_{3/2}^2$, etc. One solution (dots) is predominantly $\sigma(d_{3/2})$ and the other (triangles) $\sigma(s_{1/2})$. Calculations based on the DSD model have been shown to provide a procedure for choosing the physical $E1$ solutions.[1,17] The solid curves in Fig. 8 are the results of such a calculation (see Sec. V below) and are in agreement with the predominantly $d_{3/2}$ solution which will be considered the preferred solution from this point on.

The large values of b_1 and the resonancelike structure seen in the plot showing $A_y(90°)$ versus neutron energy suggest the presence of $M1$ radiation. Moreover, since the giant quadrupole resonance is expected to occur at an excitation energy in ^{14}C near 20–22 MeV, it is not possible to neglect, *a priori*, $E2$ radiation. With six complex T-matrix elements the problem is clearly underdetermined, and some simplifying assumptions must be made. Since calculations based on the DSD model (see Sec. V below) indicate that both the $p_{3/2}(E2)$ and $p_{1/2}(M1)$ matrix elements are at least ten times smaller than the $f_{5/2}(E2)$ and the $p_{3/2}(M1)$ matrix elements, respectively,

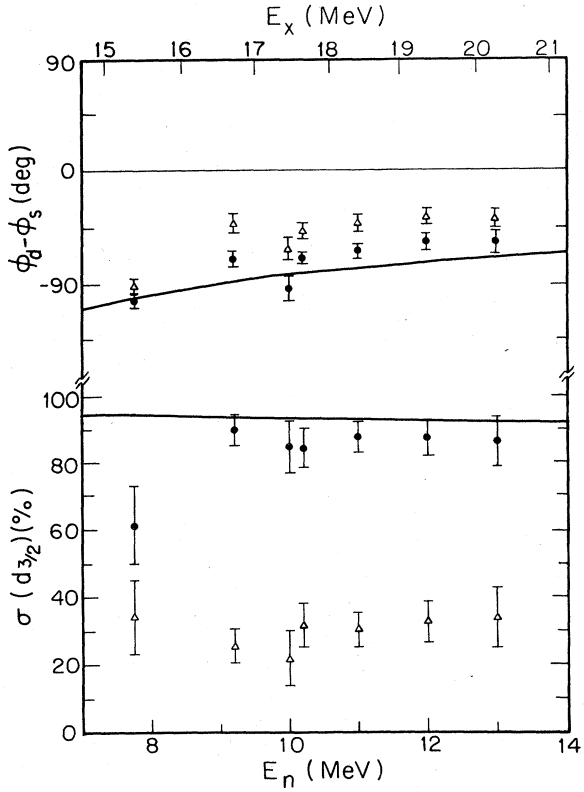

FIG. 8. The results of a pure $E1$ transition matrix element analysis of the angular distributions data obtained with the $^{13}C(\vec{n},\gamma_0)^{14}C$ reaction. Statistical uncertainties are indicated. The bottom plot shows the percentage of the $E1$ cross section due to the $d_{3/2}$ term. The upper plot shows the relative phase between the two $E1$ terms. The curves are the results of calculations described in the text.

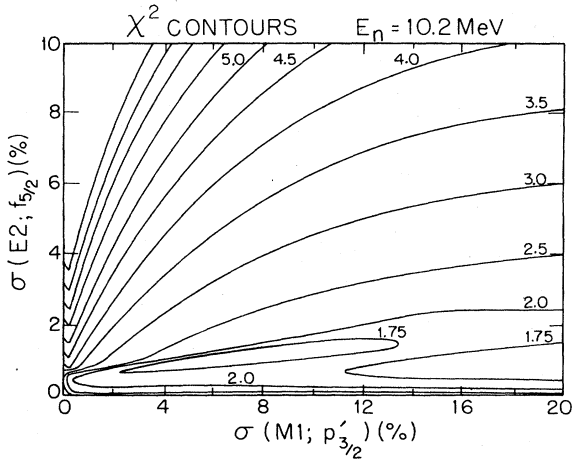

FIG. 9. A contour plot of reduced χ^2 as a function of $E2$ and $M1$ cross sections obtained from analysis (see the text) of the $E_n = 10.2$ MeV $^{13}C(\vec{n},\gamma_0)^{14}C$ data.

the $p_{3/2}(E2)$ and $p_{1/2}(M1)$ amplitudes were assumed to be zero. The T-matrix analysis was then performed at each energy by varying the $p_{3/2}(M1)$ and $f_{5/2}(E2)$ amplitudes in 24 steps such that the $M1$ partial cross section varied from 0% to 20% and the $E2$ partial cross section varied from 0% to 10% of the total cross section. The two $E1$ amplitudes and the three relative phases were determined using a search code which produced a minimum χ^2 at each of the 576 values of $p_{3/2}$ and $f_{5/2}$. Figure 9 shows, as an example, a contour plot of the reduced χ^2 values obtained from the $E_n = 10.2$ MeV angular distributions. The broad "valley" of low χ^2 indicates only that $\sigma(E2)$ is less than 2% of the total cross section and that $\sigma(M1)$ is nonzero but essentially undetermined. The results at other neutron energies were similar, so that the conclusions from the T-matrix analysis are that for excitation energies from 15.4 to 20.2 MeV the $E2$ cross section is less than 2% of the total and that $M1$ radiation is present in the $^{13}C(n,\gamma_0)$ reaction. A more detailed interpretation of the data will be made on the basis of the direct-semidirect model.

V. DIRECT-SEMIDIRECT MODEL CALCULATIONS

The direct-semidirect reaction model[3,4,18–20] has been used widely and successfully to describe many features of fast-nucleon capture data.[1,2,21] In this model, the transition amplitude is expressed as a coherent sum of two terms.[3] The direct term represents the process in which the incident particle undergoes a radiative transition to a single-particle final state. The radial part of this direct term is given by

$$\langle u_b(r) \mid d^L \mid \chi^{(+)}(r) \rangle ,$$

where u_b is the radial wave function of the captured particle in the final state, and $\chi^{(+)}$ is the continuum state radial wave function calculated from an optical model potential. The factor d^L represents the radial part of the single-particle electromagnetic operator for radiation of multipolarity L. In the long wavelength limit this operator is proportional to r^L for electric radiation and has no radial dependence for the case of magnetic dipole radiation. The other type of term (semidirect) represents a two-step process in which the incoming nucleon inelastically excites the target nucleus into a collective state while occupying the same final state as in the direct process. The collective state subsequently decays by γ-ray emission. The radial part of the semidirect amplitude is calculated according to

$$\langle u_b \mid h^L(r) \mid \chi^{(+)} \rangle / (E - E_R + i\Gamma/2) ,$$

where $h^L(r)$ is the form factor responsible for the inelastic excitation of the collective state by the incoming nucleon, and E_R and Γ refer to the position and width, respectively, of the resonance. In the present work the form factor was assumed to have a volume shape for electric dipole transitions and was written as

$$h^{E1}(r) \propto V_1 r f(r) ,$$

where V_1 is the real part of the symmetry term in the optical potential and $f(r)$ is the Woods-Saxon form factor given by

$$f(r) = \{1 + \exp[(r - r_0 A^{1/3})/a]\}^{-1} .$$

The value of V_1 was taken to be 68 MeV, while the geometry factors were taken from the optical-model parameter set of Watson *et al.*[22] which was used throughout this work. The form factor for the isoscalar quadrupole semidirect term was taken to have a surface-peaked shape and was written as

$$h^{E2}(r) \propto -r V_0 \frac{df(r)}{dr} ,$$

where $V_0 = -53$ MeV is the strength of the real central potential. The isovector giant quadrupole resonance, which should lie at an excitation energy higher than those studied here, was not included in our calculations. The $M1$ semidirect term was taken from the work of Saporetti and Guidotti[20] and was derived with the assumption that the magnetic dipole operator is *pure* isovector. The radial part of the form factor is written as

$$h^{M1}(r) \propto V_{11} f(r) .$$

The value of the interaction $V_{11} = 40$ MeV suggested in Ref. 20 was obtained from an estimate made by Bohr and Mottelson[23] based on observed magnetic moments in the neighborhood of ^{208}Pb. A recently reported value[24] of $V_{\sigma\tau} = 220$ MeV fm^3, which was deduced from studies of the giant Gamow-Teller states in medium and heavy nuclei, suggests $V_{11} \simeq (220)\bar{\rho}_+ \simeq 35$ MeV, where the average nucleon density $\bar{\rho}_+ \simeq A/(4\pi R^3/3)$. This value is in reasonable agreement with the Bohr and Mottelson estimate. The calculations reported here use $V_{11} = 40$ MeV.

The computer code HIKARI (Ref. 25) was used to perform the DSD model calculations for the $^{13}C(n,\gamma_0)^{14}C$ reaction. As mentioned above, the optical model parameters of Ref. 22 were used throughout, and the strength of the real central potential was adjusted to give the correct binding energy of the final state. The spectroscopic factor

$C^2S=1.73$ was taken from Cohen and Kurath,[26] and the recoil effective charges were taken from Ref. 7. A convolution integral was included in the calculations to account for the energy spread of the incident neutron beam.

Two uncoupled $E1$ resonances (plus direct $E1$) were included in the calculations in order to approximate the general shape of the 90° yield curve above $E_x \simeq 15$ MeV. The cross section below 15 MeV is assumed to be due to compound nuclear reactions which are not included in the model calculations. The solid curve in Fig. 3 shows the results for the $E1$ parameters $E_R(\text{MeV})/\Gamma(\text{MeV})/\eta(\%)=15.45/1.5/26$ and 17.85/1.75/25, respectively, where η is the value of the collective dipole matrix element expressed as a percentage of the dipole sum.

The results of expanded calculations which include direct $M1$ and direct $E2$ plus two narrow $M1$ resonances with the parameters $E_R(\text{MeV})/\Gamma(\text{keV})/B(M1)\downarrow = 16.7/200/0.24\mu_0^2$ and $17.5/200/0.17\mu_0^2$ are shown in Figs. 5, 6, and 7. The calculated curves have had the energy spread of the incident neutron beam folded in (approximately 300 keV near $E_x=17$ MeV). The $M1$ resonance parameters were optimized to fit the energy dependence of $A_y(90°)$ and the agreement between the calculations and the $A_y(90°)$ data is excellent throughout the excitation energy region studied. In addition, the features of the fore-aft asymmetry versus energy curve as well as the a_k and b_k coefficients are also reproduced. The $M1$ cross section is too small to be observed in the calculated 90° yield curve (Fig. 3). The addition of an isoscalar $E2$ resonance to the calculation (not shown) with the parameters $E_R(\text{MeV})/\Gamma(\text{MeV})/\eta(\%)=20/4/40$, which are typical of this mass region,[27] did not improve the fits in any significant way. Here η represents the percentage of the isoscalar $E2$ energy-weighted sum rule (EWSR) exhausted by the quadrupole matrix elements. Calculations were also made with the two $M1$ resonances replaced by two isoscalar $E2$ resonances with the parameters $E_R(\text{MeV})/\Gamma(\text{keV})/\eta(\%)=16.7/200/30$ and 17.5/200/23. The results are shown as dotted lines in Figs. 6 and 7. As before, the parameters were chosen to give the best fit to $A_y(90°)$ as a function of energy, and qualitative agreement is obtained although the large EWSR fraction required would be surprising for this small excitation energy range.[27] Moreover, the fit to the a_s data taken as a function of energy shows a substantial disagreement with the data. These results support a spin and parity assignment of 1^+ to the two narrow resonances at 16.7 and 17.5 MeV in ^{14}C.

One other 1^+ state is known[28] in ^{14}C with $E_x=11.3$ MeV and an $M1$ strength of $0.41\mu_0^2$ ($\Gamma_\gamma=6.8$ eV, Ref. 29). Thus, the $M1$ strength in ^{14}C appears to be fragmented. This fragmentation is similar to that observed in other light nuclei[30] when two nucleons are added to a "self-conjugate core."

The accuracy of the total $M1$ strength obtained from this work is limited by several factors. Experimentally, the large energy spread of the incident neutron beam makes it difficult to accurately determine the widths of the narrow resonances. Equally good fits can be obtained with widths that varied from 100 to 250 keV and with corresponding changes in the $B(M1)$ values. Higher resolution measurements would help but must await the availability of high-current pulsed polarized-deuteron beams which will allow lower pressures in the deuterium gas cell. A more serious problem may be the question of whether the DSD model (including the assumed $V_{11}=40$ MeV) is appropriate for describing the excitation of such narrow ($\Gamma \simeq 200$ keV) isovector $M1$ states. The resolution of this problem will require more theoretical and experimental work.

VI. SUMMARY

The $^{13}C(n,\gamma_0)^{14}C$ reaction has been studied with polarized and unpolarized neutrons for the excitation energy range of 13.4 to 24.0 MeV. The amplitudes and relative phase of the two $E1$ T-matrix elements were determined, and they show two classes of solutions—one predominantly $d_{3/2}$ and the other predominantly $s_{1/2}$. A direct-semidirect model calculation suggests that the case with $\sigma(d_{3/2})$ accounting for about 85% of the $E1$ cross section is the physical solution. An expanded analysis, which assumed only one $E2(f_{5/2})$ and one $M1(p_{3/2})$ T-matrix element, did not yield unique solutions but did set a limit on the $E2$ cross section at less than 2% of the total cross section for those excitation energies for which angular distributions were measured. The measured values of the b_1 coefficient and the energy dependence of the 90° analyzing power indicated two narrow resonancelike structures near 17 MeV excitation energy. When these data were compared with the results of direct-semidirect model calculations, it was concluded that these structures are due to two $M1$ resonances having excitation energies of 16.5 and 17.5 MeV with $B(M1)$ values of $0.24\mu_0^2$ and $0.17\mu_0^2$, respectively. The widths of both resonances are about 200 keV. Although the existence of these $M1$ states is quite clear, the model dependent extraction of their strengths leaves these parameters rather uncertain.

ACKNOWLEDGMENTS

The authors are grateful to J. W. Jury for the loan of the ^{13}C target. This work was supported by the U.S. Department of Energy Director of Energy Research, Office of High Energy and Nuclear Physics, under Contract No. DE-AC05-76ER01067.

*Permanent address: Research Laboratory for Nuclear Reactors, Tokyo Institute of Technology, Tokyo, Japan.

[1]H. R. Weller and N. R. Roberson, Rev. Mod. Phys. **52**, 699 (1980).

[2]K. A. Snover, in *Neutron Capture Gamma-Ray Spectroscopy*, edited by R. E. Chrien and W. R. Kane (Plenum, New York, 1978), p. 319.

[3]G. E. Brown, Nucl. Phys. **57**, 339 (1964).

[4]C. F. Clement, A. M. Lane, and J. A. Rook, Nucl. Phys. **66**, 273 (1965); **66**, 293 (1965).

[5]M. Jensen, D. R. Tilley, H. R. Weller, N. R. Roberson, S. A. Wender, and T. B. Clegg, Phys. Rev. Lett. **43**, 609 (1979).
[6]E. D. Arthur, D. M. Drake, and I. Halpern, Phys. Rev. Lett. **35**, 914 (1975).
[7]B. Buck and A. A. Pilt, Nucl. Phys. **A280**, 133 (1977).
[8]H. R. Weller and N. R. Roberson, IEEE Trans. Nucl. Sci. **NS-28**, 1268 (1981).
[9]S. E. King, N. R. Roberson, and S. A. Wender, Bull. Am. Phys. Soc. **26**, 90 (1981).
[10]M. Drosg, Nucl. Sci. Eng. **67**, 180 (1978).
[11]P. W. Lisowski, R. L. Walter, C. E. Busch, and T. B. Clegg, Nucl. Phys. **A242**, 298 (1975).
[12]T. A. Trainer, T. B. Clegg, and P. W. Lisowski, Nucl. Phys. **A220**, 533 (1974).
[13]P. Paul, in *Nuclear Spectroscopy and Reactions,* Part A, edited by J. Cerny (Academic, New York, 1974), p. 345.
[14]E. Hayward, in *Photonuclear Reactions,* National Bureau of Standards Monograph 118 (U.S. Department of Commerce, Washington, D.C., 1976), p. 38.
[15]H. R. Kissener, R. A. Eramzhian, and H. U. Jager, Nucl. Phys. **A207**, 78 (1973).
[16]S. S. Hanna, H. F. Glavish, E. M. Diener, J. R. Calarco, C. C. Chang, R. Avida, and R. N. Boyd, Phys. Lett. **40B**, 631 (1972).
[17]H. R. Weller, N. R. Roberson, and S. R. Cotanch, Phys. Rev. C **18**, 65 (1978).
[18]G. Longo, F. Saporetti, and R. Guidotti, Nuovo Cimento **46A**, 509 (1978), and references therein.
[19]A. Likar, M. Potokar, and F. Cvelbar, Nucl. Phys. **A280**, 49 (1977), and references therein.
[20]F. Saporetti and R. Guidotti, Nucl. Phys. **A311**, 284 (1978), and references therein.
[21]I. Bergqvist and M. Potokar, in *Neutron Capture Gamma-Ray Spectroscopy,* edited by R. E. Chrien and W. R. Kane (Plenum, New York, 1979), p. 299.
[22]B. A. Watson, P. P. Singh, and R. E. Segel, Phys. Rev. **182**, 977 (1969).
[23]A. Bohr and B. R. Mottelson, *Nuclear Structure* (Benjamin, New York, 1979), Vol. II, p. 638.
[24]H. Toki, D. Cha, and G. Bertsch, Phys. Rev. C **24**, 1371 (1981).
[25]H. Kitazawa, private communication.
[26]S. Cohen and D. Kurath, Nucl. Phys. **A101**, 1 (1967).
[27]F. E. Bertrand, Annu. Rev. Nucl. Sci. **26**, 457 (1976).
[28]F. Ajzenberg-Selove, Nucl. Phys. **A268**, 1 (1976).
[29]H. Crannell, J. M. Finn, P. Hallowell, J. T. O'Brien, N. Ensslin, L. W. Fagg, E. C. Jones, and W. L. Bendel, Nucl. Phys. **A278**, 253 (1977).
[30]L. W. Fagg, Rev. Mod. Phys. **47**, 683 (1975).